

## The progenitor and remnant of the helium nova V445 Puppis

V. P. Goranskij<sup>1</sup>, S. Yu. Shugarov<sup>1,2</sup>, A. V. Zharova<sup>1</sup>, P. Kroll<sup>3</sup>, and E. A. Barsukova<sup>4</sup>

<sup>1</sup> Sternberg Astronomical Institute, Moscow University, Universitetsky Ave. 13, Moscow, 199992 Russia

<sup>2</sup> Astronomical Institute of the Slovak Academy of Sciences, Tatranska Lomnica, 05960 Slovakia

<sup>3</sup> Sternwarte Sonneberg, Sternwartestrasse 32, Sonneberg, D-96515 Germany

<sup>4</sup> Special Astrophysical Observatory, Russian Academy of Sciences, Nizhny Arkhyz, Karachai-Cherkesia, 369167 Russia

V445 Pup was a peculiar nova with no hydrogen spectral lines during the outburst. The spectrum contained strong emission lines of carbon, oxygen, calcium, sodium, and iron. We have performed digital processing of photographic images of the V445 Pup progenitor using astronomical plate archives. The brightness of the progenitor in the *B* band was  $14^m3$ . It was a periodic variable star, its most probable period being  $0^d.650654 \pm 0^d.000011$ . The light curve shape suggests that the progenitor was a common-envelope binary with a spot on the surface and variable surface brightness. The spectral energy distribution of the progenitor between 0.44 and 2.2  $\mu\text{m}$  was similar to that of an A0V type star.

After the explosion in 2001, the dust was formed in the ejecta, and the star became a strong infrared source. This resulted in the star's fading below  $20^m$  in the *V* band. Our CCD *BVR* observations acquired between 2003 and 2009 suggest that the dust absorption minimum finished in 2004, and the remnant reappeared at the level of  $18^m5$  *V*. The dust dispersed but a star-like object was absent in frames taken in the *K* band with the VLT adaptive optics. Only expanding ejecta of the explosion were seen in these frames till March 2007. No reddened A0V type star reappeared in the spectral energy distribution. The explosion of V445 Pup in 2000 was a helium flash on the surface of a CO-type white dwarf. Taking into account the results of modern dynamic calculations, we discuss the possibility of a white-dwarf core detonation triggered by the helium flash and the observational evidence for it. Additionally, the common envelope of the system was lost in the explosion. Destruction in the system and mass loss from its components exclude the future SN Ia scenario for V445 Pup.

## 1 INTRODUCTION

The outburst of V445 Pup was discovered on 30 December 2000 by Kanatsu (Kato & Kanatsu 2000). The earliest observation of V445 Pup in the outburst, dated 19 November 2000, was found in the ASAS archive. At that time, the brightness of the star was  $8^m8$ . The brightness maximum of  $8^m46$  in the *V* band was reached on 29 November 2000. The first spectroscopic observations in the outburst by Wagner et al. (2001) showed that the Balmer emission and He I lines typical of classical novae were not present in the spectrum of V445 Pup. The spectra were dominated by emission lines arising from FeII, CaII, CII, NaI, OI. Line widths corresponded to an expansion velocity of about  $1000 \text{ km s}^{-1}$ . The ejecta produced during the outburst allow us to consider V445 Pup as a nova.

The nature of classical novae is known to be a thermonuclear explosion of hydrogen on the surface of a white dwarf in a semidetached binary system. Hydrogen accumulates on the surface of the white dwarf due to accretion from a donor, usually a red dwarf. As a result of hydrogen explosion, strong Balmer lines are observed in the spectra of classical novae. Ashok & Banerjee (2003) suggested that V445 Pup was the unique helium nova predicted theoretically by Kato et al. (1989) and by Iben & Tutukov (1994) who considered the case of a degenerate white dwarf accreting helium from a helium-rich donor. Note that a subclass of classical novae called helium-nitrogen (He/N) novae was

introduced by Williams (1992). These novae have spectra with strong Balmer lines, and they also have HeI and HeII lines. CNO elements seen in the spectra were mixed by accumulated hydrogen envelope from the surface of the white dwarf through a dredge-up mechanism (for instance, cf. Glasner & Livne 2002). The case of helium nova suggests that the donor is a nucleus of an evolved star that previously lost its hydrogen envelope due to accretion.

In the outburst of V445 Pup, the decay of brightness by  $1^m8$  continued gradually for 164 days and was followed by a small rebrightening between 12 May and 21 June 2001. The last observation of V445 Pup in the outburst was on 11 July 2001 at visual magnitude 11.5. Then the star faded rapidly and was not seen in August 2001. On 4 October 2001, no object brighter than  $V = 20^m$  or  $I = 19^m5$  was found by Henden et al. (2001) at the position of V445 Pup. They remark: “The object is evidently shrouded in a thick and dense carbon dust shell, in view of the apparent over-abundance of carbon in ejecta previously observed in infrared and optical spectra”. Lynch et al. (2001) detected the infrared radiation in the 3–14  $\mu\text{m}$  range just 1 month after the object had been discovered. The spectrum revealed smooth and featureless continuum, which they treated as a thermal emission of dust with the temperatures ranged between 280 and 1300 K. They suggest that this dust was a product of previous outbursts, at least in part.

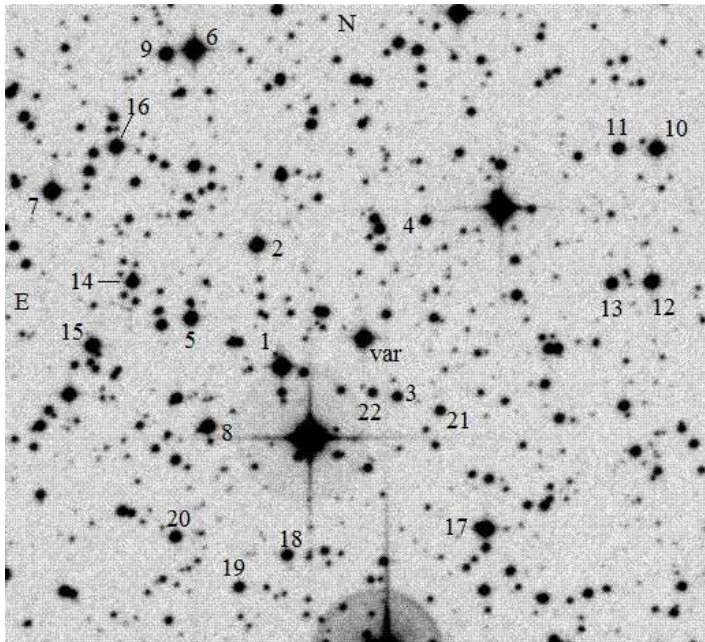


**Figure 1.** The finding chart of V445 Pup and comparison stars. This is a copy of a digitized image obtained with the UKST Schmidt telescope on 4 April 1980 on IIIaJ emulsion with a GG 395 filter. The progenitor is indicated as “var”.  $V$  magnitudes, colour indices of marked stars, and corresponding uncertainties (in units of thousandths of a magnitude) are given in Table 1.

The detailed spectral evolution of V445 Pup in the outburst was studied by Iijima & Nakanishi (2008). They acquired high- and medium-resolution spectra for the optical wavelengths 3900–7000  $\text{\AA}$ . They confirmed the absence of hydrogen lines and noted unusually strong emissions of carbon ions. Some metal lines had P Cyg profiles with absorption components blue-shifted roughly by  $-500 \text{ km s}^{-1}$ ; this velocity was assumed to be the outflow velocity. The cited authors measured large radial velocity of V445 Pup,  $+224 \pm 8 \text{ km s}^{-1}$ , which suggested that the object belonged to the old disk population.

The distance was estimated from the interstellar NaI D<sub>1</sub> and D<sub>2</sub> absorption lines to be  $3.5 < d < 6.5$  kpc; the reddening is  $E(B - V) = 0.51$ .

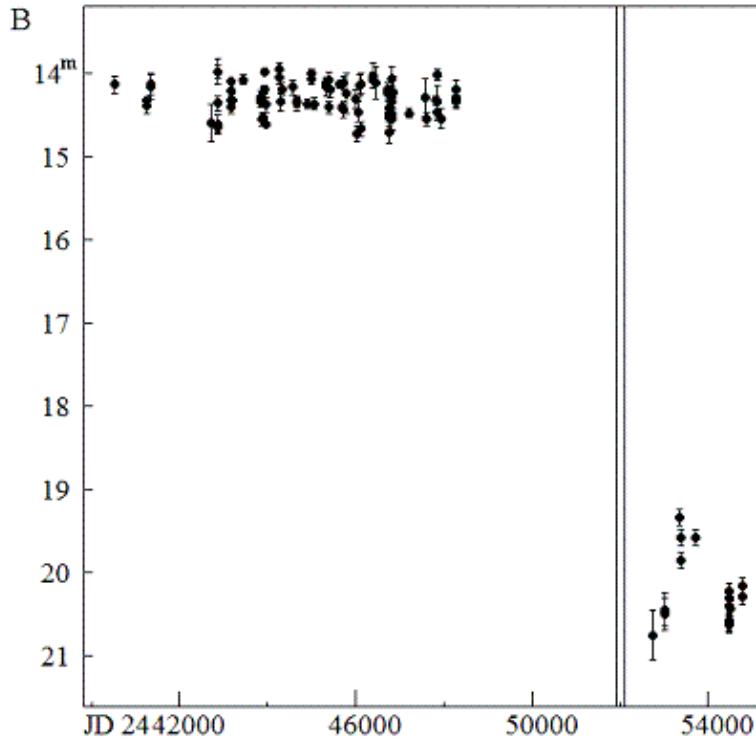


**Figure 2.** The pre- and post-outburst light curve of V445 Pup in the  $B$  band. The start and the end of the 2000–2001 outburst are indicated with a double vertical line.

Lynch et al. (2004) reported that in January, 2004 the object had faded to fainter than  $J = 18$ , so that they could not take its spectrum in the visible range. In the infrared, they detected only two HeI lines at  $1.0830$  and  $2.0581 \mu\text{m}$ , both showing doubled profiles due to bipolar outflow. The very red continuum was detected only at  $\lambda \geq 1.5 \mu\text{m}$ . It was produced by emission of hot dust.

Woudt et al. (2009) published the results of post-outburst  $JHK$  photometry, adaptive optics imaging in the  $K$  band, and optical-range spectroscopy of V445 Pup. They discovered an expanding and narrowly confined bipolar shell, the outflow characterized by large velocity of  $6720 \pm 650 \text{ km s}^{-1}$ . Some knots were moving with larger velocities,  $8450 \pm 570 \text{ km s}^{-1}$ . They derived an expansion parallax distance of  $8.2 \pm 0.5$  kpc. They noted that the expansion velocity measured by Iijima & Nakanishi (2008) from their high-resolution spectra in the outburst was only  $500 \text{ km s}^{-1}$ . Such a big difference may be due to strong collimation of bipolar ejection located just in the plane of the sky and inclined to this plane by only  $5^{\circ}8 - 3^{\circ}7$  (Woudt et al. 2009). The authors assume that the small inclination angle may confirm the presence of an orthogonal dust structure closely aligned to the line of sight and causing the strong extinction observed after the outburst. In their spatially resolved optical spectrum obtained with the VLT in January, 2006 in the  $4465\text{--}7634 \text{ \AA}$  range, only the emission lines of [OI], [OII], [OIII], and HeI were seen, but not the continuum.

The presence of a bright progenitor of V445 Pup having a visual magnitude of  $13.1$  was first noted by Platais et al. (2001). Its absolute proper motion was small,  $\mu = 0''.008 \pm 0''.004$ . With the distance derived by Woudt et al. (2009), the luminosity of

the progenitor proved to be very large,  $\log L/L_\odot = 4.34 \pm 0.36$ , which is consistent with the absolute bolometric magnitude  $M_{bol} = -6.1 \pm 0.9$ . Woudt et al. (2009) note that the derived luminosity suggests that V445 Pup probably contains a massive white dwarf accreting at a high rate from a helium star companion. But they did not exclude that the companion was also a bright star. Liller (2001) reminded of three hydrogen-deficient cataclysmic variables, CR Boo, CP Eri, and V803 Cen, all of them hot blue objects showing no hydrogen but revealing HeI emission lines. The absolute magnitude of  $-6.1$  is unprecedented high for a cataclysmic variable, making us to think about the nature of the progenitor.

The observations of the light curve in the outburst and light curve modeling by Kato et al. (2008) reveal that the CO white dwarf in V445 Pup is very massive and close to the Chandrasekhar mass limit ( $M_{wd} \geq 1.35M_\odot$ ); a half of the accreted matter remained on the white dwarf after the outburst. Therefore, V445 Pup was considered a strong candidate for a type Ia supernova progenitor. P. Woudt and D. Steeghs called V445 Pup a “ticking stellar time bomb” in the ESO Science Press Release 0943. Taking into account the observations with adaptive optics by Woudt et al. (2009) which show only spatially resolved products of eruption but no stellar component, it is hard to maintain the concept that the mass of the system increases. The question is what mass of the components was left after the explosion.

The scenario for V445 Pup may be quite different. Recent dynamic 3D simulations by Guillochon et al. (2010) discovered a new mechanism for the detonation of a core of a sub-Chandrasekhar CO white dwarf (with a mass lower than  $1.4M_\odot$ ) in a system with a pure He white dwarf or a He/CO hybrid secondary. Fink et al. (2010) found that secondary core detonations were triggered for all of the simulated models ranging in core mass from 0.810 up to  $1.385M_\odot$  with corresponding helium shell masses from 0.126 down to  $0.0035M_\odot$ . In that paper, the double detonation scenario remains a potential explanation for type Ia supernovae. But the destruction of the CO white dwarf means that V445 Pup, after its outburst in 2000, will not be a type Ia supernova progenitor. It is of great interest if the narrowly confined bipolar cones observed by Woudt et al. (2009) are debris of the detonated white dwarf. The overabundant carbon in the outburst will also be an evidence for CO white dwarf detonation.

Fortunately, there are many photographic images of V445 Pup in the world astronomical plate collections suitable for resolving the puzzle of the progenitor. Woudt et al. (2009) verified the plate archives at the Harvard–Smithsonian Center for Astrophysics (USA) and found no prior outbursts in 1897–1955. The progenitor of V445 Pup was identified on many plates at approximately constant brightness (from visual comparison with surrounding stars). We found many plates in archives of the Sternberg Astronomical Institute (SAI) of the Moscow University (Russia) and in archives of the Sonneberg Observatory (Germany). Two of us (V.P.G. and S.Yu.Sh.) performed eye estimates of V445 Pup, V.P.G. for Moscow plates, and S.Yu.Sh. for Sonneberg plates. The two sets showed similar behavior and marginal variability. But unexpectedly, the preliminary frequency analysis revealed the same periodicity in both sets with the period of 0<sup>d</sup>.650653, coinciding to the 6th significant digit. Both light curves were of low quality. Therefore we decided to digitize the images of V445 Pup and to perform digital processing.

## 2 OBSERVATIONS AND DATA PROCESSING

In the Moscow SAI plate collection, we found 51 plates with images of V445 Pup taken with the SAI Crimean Station 40-cm f/4 astrograph and dated between 15 November

1969 and 4 November 1989. AGFA ASTRO and ORWO ZU-2 photographic plates, produced in the former GDR and having high sensitivity in blue light, were used, the exposure times were 45 minutes. The geographic position of the SAI Crimean Station is  $2^{\text{h}}16^{\text{m}}08^{\text{s}}, +44^{\circ}43'42''$ . The declination of V445 Pup is about  $-26^{\circ}$ . This means that the highest altitude of the star above the horizon is  $19^{\circ}$ . The observations were limited to a 3-hour visibility time around this point. The photographic plates were mostly centered at  $\tau$  CMa, they cover an area of  $10^{\circ} \times 10^{\circ}$ . The region of about  $20' \times 20'$  centered at V445 Pup was digitized for each plate using the SAI CREO EverSmart Supreme scanner. CREO scanner frames are in the TIFF format.

We found 56 measurable images of V445 Pup on the plates of the Sonneberg Observatory collection dated between 19 March 1984 and 17 January 1991. These plates were taken with the 40-cm f/4 astrograph having optics basically similar to that of the SAI Crimean Station astrograph. Also, plates of basically the same type produced in the former GDR were used, so all our photographic material is very uniform. The Sonneberg Observatory has the geographic position  $0^{\text{h}}44^{\text{m}}46^{\text{s}}, +50^{\circ}22'39''$ , it is about  $5^{\circ}$  to the north by latitude compared to the SAI Crimean Station. Thus, the star rises only to  $14^{\circ}$  for this geographic point, and its visibility time is less than that for the Crimean Station. Sky images are evidently affected with variable atmospheric extinction across the plate field. In these plates, the star is located near the center. The typical exposure time for these plates is 20 minutes. Images of V445 Pup were digitized using the Fuji FinePix F10 CCD camera and an ordinary biconvex lens. Frames made with this camera are in the JPEG format. After several experiments, we found that this method of digitizing gave the quality of measurements near the field center as good as that of a scanner. To increase the S/N ratio, we co-added several subsequent frames in night series. The frames were combined with matching two stars and with the field rotation. The combined exposures of co-added frames were between 40 and 60 minutes. The total number of measurements for the star, including co-added ones, is 31.

Additionally, we measured all the Internet-accessible Digital Sky Survey images of V445 Pup in  $B$ ,  $R$ , and  $I$  bands and used 2MASS  $JHK$  magnitudes to study the spectral energy distribution of the progenitor.

All the frames were processed in the Windows BITMAP format. Extraction of images was made using the aperture method with star-profile correction; the WinPG software developed by V.P.G. was utilized. Special software was written by V.P.G. to approximate the characteristic curves with an  $n$ th-degree polynomial, with graphical output. Practically, approximations with  $n = 1$  or  $2$  were optimal. The total number of comparison stars used to build a characteristic curve was 23; a few stars with the largest deviations were eliminated from calculations, and the characteristic curves were re-calculated in such cases. The r.m.s. deviation of comparison stars from the polynomial fit was formally taken for the uncertainty of V445 Pup measurement.

Carrying out our photographic measurements, we used the CCD  $BVR_cI_c$  standard sequence in the vicinity of V445 Pup published by A. Henden for VSNET. We present the finding chart of the progenitor in Fig. 1. The standard stars chosen by us are also marked in this Figure. We give Henden's magnitudes and their uncertainties for the chosen comparison stars in Table 1 because they are no longer accessible at the VSNET address.

The Moscow archive observations of the V445 Pup progenitor are presented in Table 2; the Sonneberg ones, in Table 3; and those from digitized sky surveys are collected in Table 4.

We performed our observations of the V445 Pup remnant between 31 March 2003 and 20 October 2009. These observations were acquired in the Special Astrophysical Observa-

tory (SAO), with the 1-m Zeiss reflector and CCD  $UBVR_CI_C$  photometer equipped with an EEV 42-40 CCD chip. The geographic position of the SAO is  $2^{\text{h}}45^{\text{m}}46^{\text{s}}, +43^{\circ}39'12''$ . The highest altitude of the star over the horizon is  $20^{\circ}$ . This object is difficult for observations and needs good sky transparency and seeing. Some constructions of the 6-m telescope dome located to the south of the 1-m reflector hamper observations of objects with such a southern declination. Additionally, a part of our observations were obtained with the SAI Crimean Station's 60-cm reflector and  $UBVR_JI_J$  photometer with the Princeton Instruments VersArray CCD. Both devices are cooled with liquid nitrogen to a temperature stabilized at  $-130^{\circ}\text{C}$ , allowing to record signals from very faint astrophysical objects. The frames were reduced in the FITS format. The extraction of images was made using the same aperture method with star-profile correction, the WinFITS software by V.P.G. was utilized. Our CCD observations are presented in Table 5.

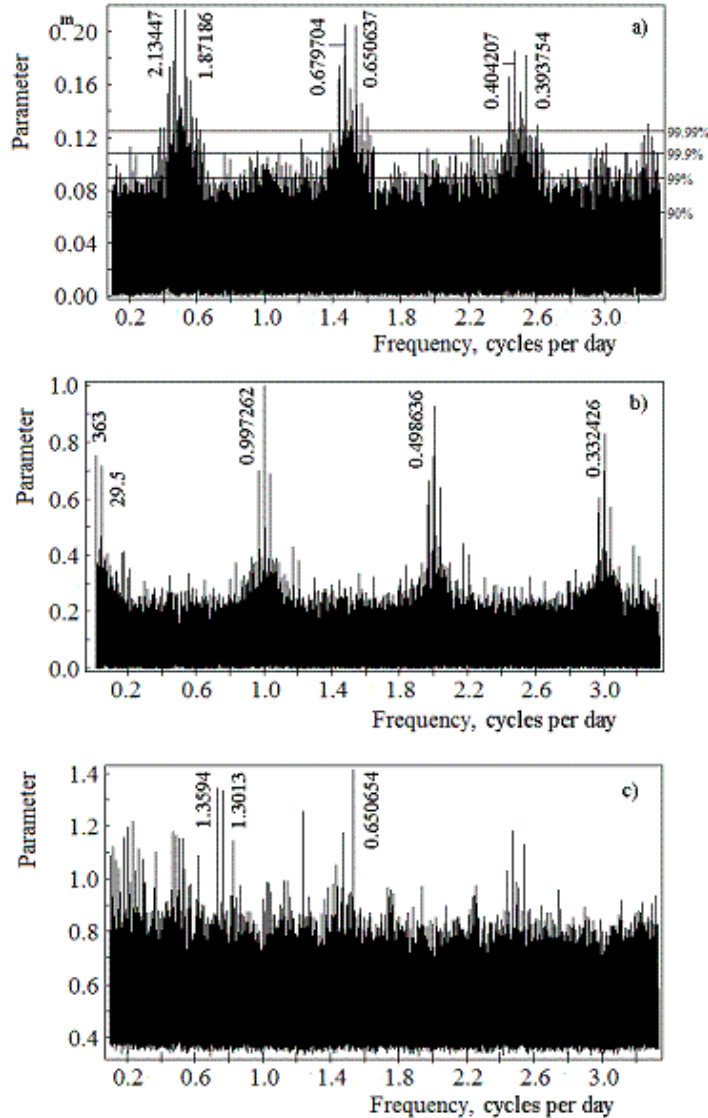


**Figure 3.** Periodograms of the V445 Pup progenitor. (a): The Deeming amplitude spectrum in the (10–0.3)-day period range. The parameter is the half-amplitude. (b): The spectral window of the same time series in the (1000–0.3)-day range. The parameter is the half-amplitude. (c): The Lafler–Kinman periodogram. The parameter is  $\theta^{-1}$ ,  $\theta$  being the normalized sum of squared magnitude differences between each two subsequent points of the phased light curve calculated with a trial period.

### 3 ANALYSIS

The light curve of V445 Pup in the  $B$  band excluding the outburst is shown in Fig. 2. The variability of the progenitor is evident, and its full amplitude exceeds the mean uncertainty of the observations more than thrice.

The frequency analysis of the progenitor observations was performed using two independent methods: (1) the discrete Fourier transform for arbitrarily distributed time series (Deeming 1975), and (2) the phase dispersion minimization (PDM) method (Lafleur & Kinman 1965). Implementations of these methods are provided with the EFFECT code developed by V.P.G. We analyzed the combined time series including Moscow and Sonneberg photographic observations. The periodograms are shown in Fig. 3a-c. The panels (a) and (b) of this figure present the amplitude spectrum and the spectral window for this series. We estimate significance levels for peaks of the amplitude spectrum using the empirical method suggested by Terebizh (1992). This method is based on a statistical analysis of simulated chaotic series generated by mixing the original series. In the chaotic series, each Julian date gets an accidental magnitude chosen from the same original series and, as a result, the chaotic series contains the same magnitudes and times. When we compute the amplitude spectrum of the chaotic series, we make more than a million of accidental light-curve implementations with arbitrary periods and estimate their amplitudes. The software provides the analysis of the cumulative probability distribution function for amplitudes in the spectrum of the chaotic series. The amplitude levels corresponding to cumulative probabilities of 90, 99, 99.9 and 99.99 percent for the chaotic series are plotted in Fig. 3a as straight lines.

The presence of strong peaks in the amplitude spectrum of the original series exceeding 99.99 percent amplitude level of the chaotic series means that the probability of casual appearance of these peaks is less than 0.01 percent. The progenitor of V445 Pup was evidently a periodic variable star. The multiplicity of peaks means that we have multiple solutions for periodicity with the Moscow and Sonneberg series.

The spectral window (Fig. 3b) demonstrates the periodicity in time discontinuities in our series amounting to the sidereal day ( $P_{sd} = 0^d.997262$ ) and to  $P_{sd}/n$ , where  $n = 2, 3, 4, \dots$ . The amplitudes of these peaks decrease when the period decreases because of increasing phase window. The phase window for  $P_{sd}$  is 0.2. Thus, for each peak in the window spectrum, we have a pair of symmetrically located alias peaks in the amplitude spectrum. The light curves corresponding to this pair of peaks have reverse phase count, so they look as mirror-reflection ones. The list of periods and frequencies of aliases is given in Table 6. One can see that the dominating peaks are sidereal-day-related. The formula of corresponding interdependence is given for each peak in the last column, ‘Remark’, of Table 6. For  $f_0$ , we chose the lowest-frequency wave with the highest amplitude. Peaks of a lunar month (29.5 day) and of about a year (363 days) in the spectrum of the window are also present, which are responsible for combs of small peaks located around the sidereal-day-related peaks in the star spectrum.

The light curves corresponding to all alias periods are given in Fig. 4. These are single-wave curves. The light curves are approximately sinusoidal, the full amplitude of the sine wave is about  $0^m.4$ . Formally, the Deeming method reveals the highest-amplitude light curves for two periods,  $1^d.871862 \pm 0^d.00009$  and  $2^d.134469 \pm 0^d.00011$ , with equal half amplitudes of  $0^m.22$ . The scatter of all the light curves reveals essential intrinsic variability. A few points do evidently contradict the sinusoidal solution. We verified these points and confirmed their Julian dates and magnitudes. These light curves may represent the case of reflection effect on the surface of a secondary star due to heating of a part of its surface by the X-ray or short-wavelength radiation coming from the primary star. However, no

X-ray source was associated with V445 Pup before its outburst. In principle, such light curves may arise due to a large hot spot on the surface of a star. FK Com-type stars may be examples of a rotating star having a hot spot on the surface. These stars are considered to be close binary systems with a common envelope.

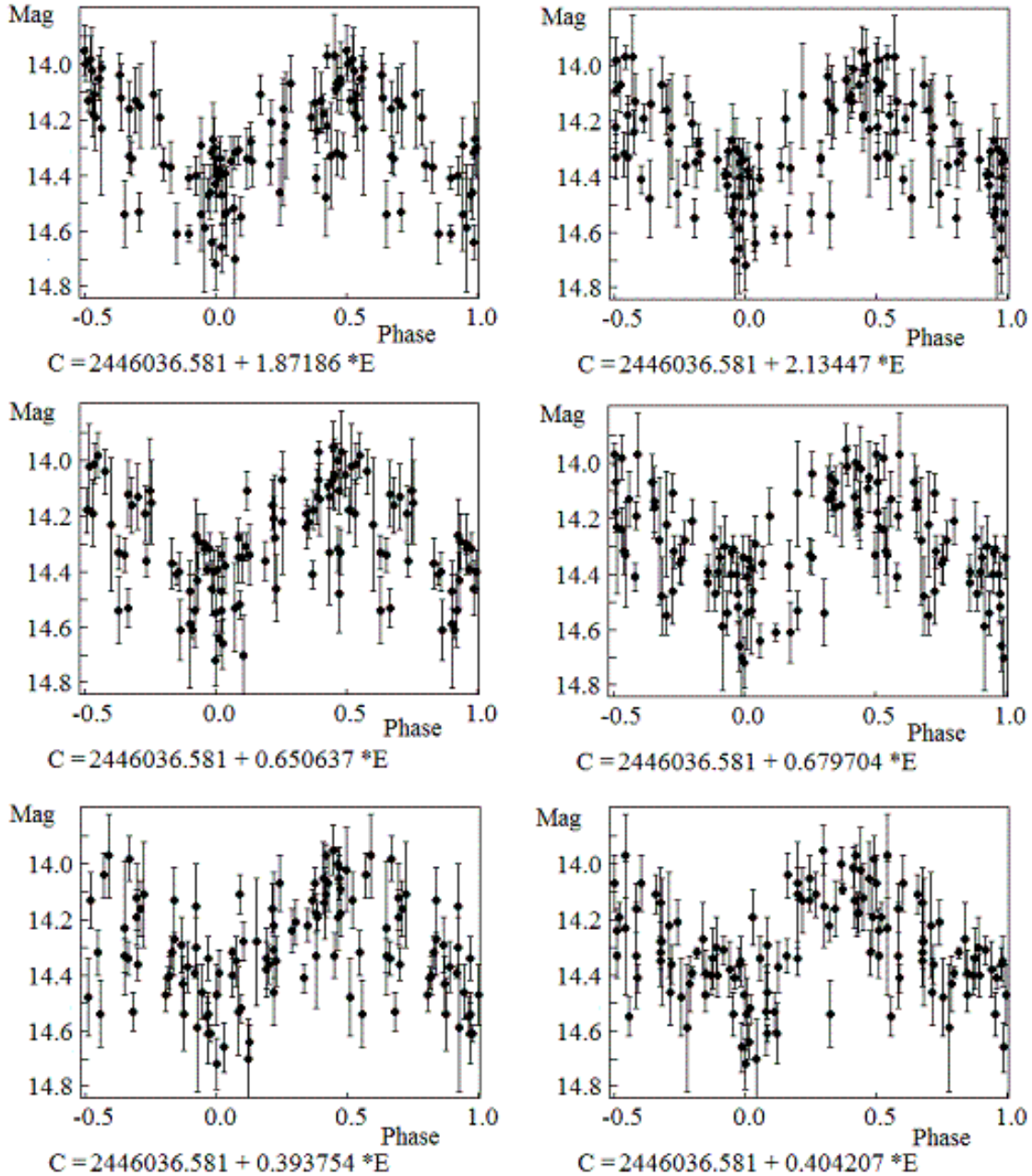


**Figure 4.** The light curves plotted for the periods determined with the Deeming (1975) method and presented in Table 6. The elements used to calculate phases are given below each curve.

Double-wave light curves for periods found by the Deeming method presented in Table 6 were also calculated and are shown in Fig. 5. Double-wave light curves are exhibited by W UMA-type binaries, these are also stars with common envelopes. In most observational cases of photometry without additional spectroscopic information, like radial velocity curves or double lines in the spectra, we can distinguish between single-wave and double-wave orbital periods only by differing alternate minima.



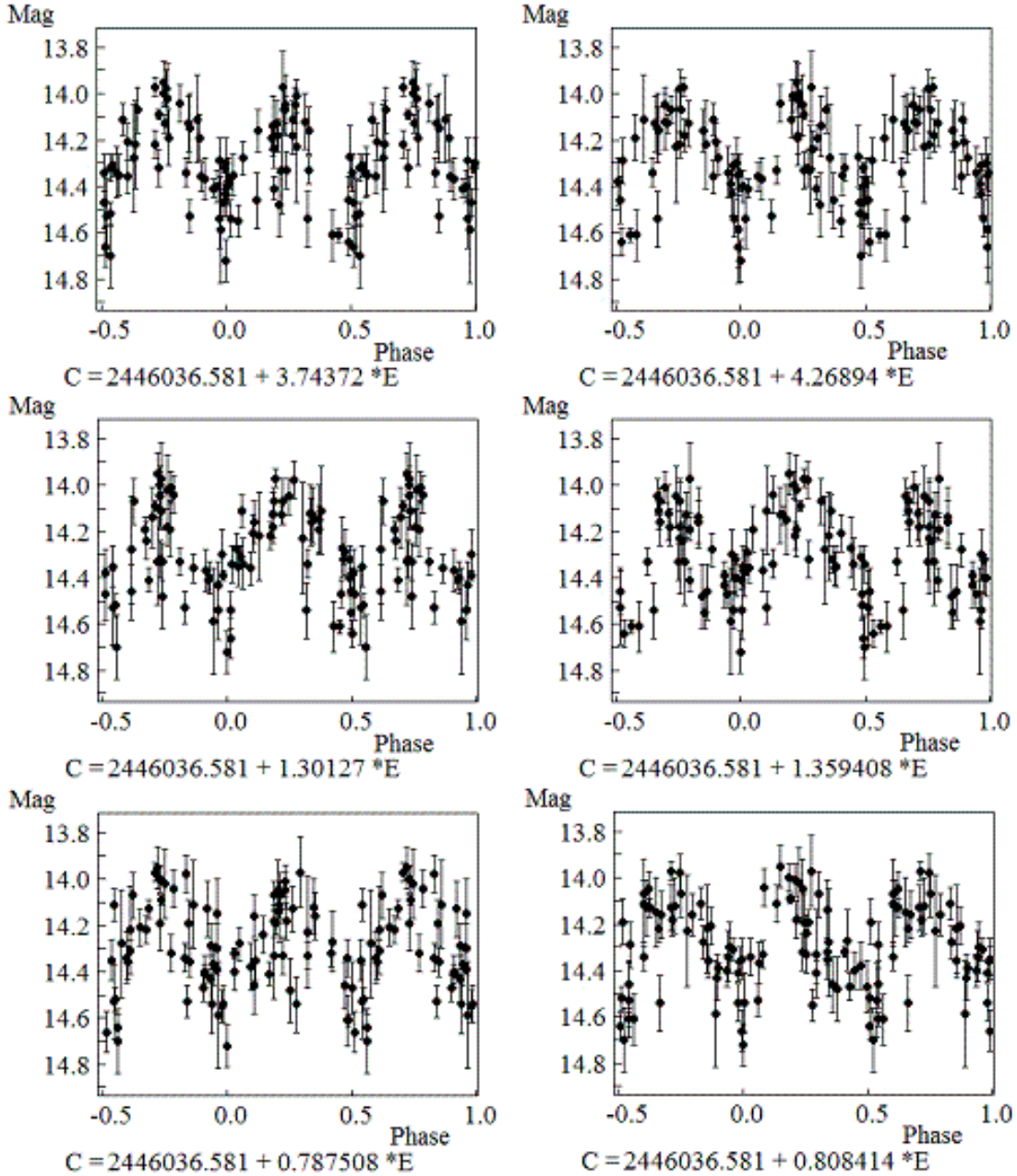


**Figure 5.** Light curves plotted for double periods determined with the Deeming (1975) method and given in Table 6. The elements used to calculate phases are given below each curve.

The difference of minima depths appears due to difference of surface brightness of the components. Our observations do not show alternate minima of different depth. Unfortunately, the accuracy of photographic observations is insufficient to make a reliable choice between single- and double-wave curves. However, taking into account that this system contains a massive accreting CO white dwarf (Kato et al. 2008), we think that a W UMa light curve is not an acceptable solution because components of such a system should have different brightness.

The Lafler–Kinman (L–K) method reveals periods not exceeding one day as preferable:  $0^d.650654 \pm 0^d.000011$ ,  $0^d.679686 \pm 0^d.000012$  day, and their double-wave aliases  $1^d.301269 \pm 0^d.000044$  and  $1^d.359423 \pm 0^d.000048$ . The 0.650654-day period determined with the L–K

method differs essentially from that determined by the Deeming method because the light curve plotted with the PDM solution shows a local detail for the phases between 0.9 and 0.1 that looks like a shallow eclipse (Fig. 6). However, additional photographic material is needed to verify if this detail is real. Certainly, a detail like a shallow eclipse cannot be revealed in a light curve with the Deeming method. The double-wave light curves found by the L–K method seem more irregular and asymmetric. Additionally, the light curve with the period of  $0^d650654 \pm 0^d000011$  is the most symmetric one and has the lowest dispersion, so we choose it as the best solution for the present time.

Our investigation shows that one can find a single final solution for the orbital period of V445 Pup only using observations acquired at different geographic longitudes, thus increasing the observational phase window of the sidereal-day period,  $P_{sd}$ . Fortunately, there are enough plates in the world plate collections to get such a solution. It is known that Harvard plates were taken at the station located in the southern hemisphere, and this series would have the widest window. We hope that digitally reduced Harvard plates and Japanese pre-outburst photographic observations, along with our data, will provide a true final solution.

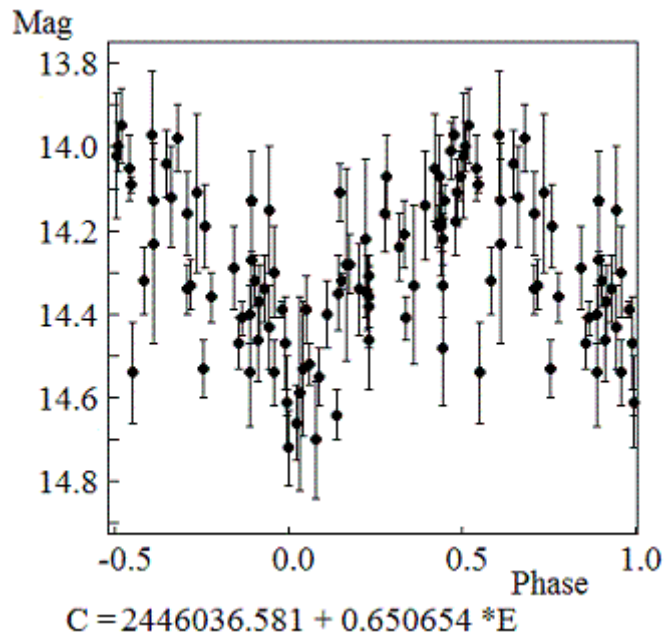


**Figure 6.** The light curve for the best single-wave period found with the Lafler & Kinman (1965) method.

## 4 SPECTRAL ENERGY DISTRIBUTIONS

We have remeasured  $B$ ,  $R$  and  $I$  frames of Digital Sky Surveys for the V445 Pup progenitor using Henden’s photometric comparison-star sequence. The infrared  $JHK$  observations of the progenitor were taken from the 2MASS survey. Additionally, we compared these observations to our optical  $BVR_CI_C$  observations of the remnant based on the same comparison-star sequence. The brightness of the remnant was found to be variable in the magnitude ranges of 19.3–20.8 in the  $B$  band; 18.5–20.3 in the  $V$  band; 17.5–19.4 in the  $R_C$  band; and 17.7–20.0 in the  $I_C$  band. In Fig. 7, we show the spectral energy

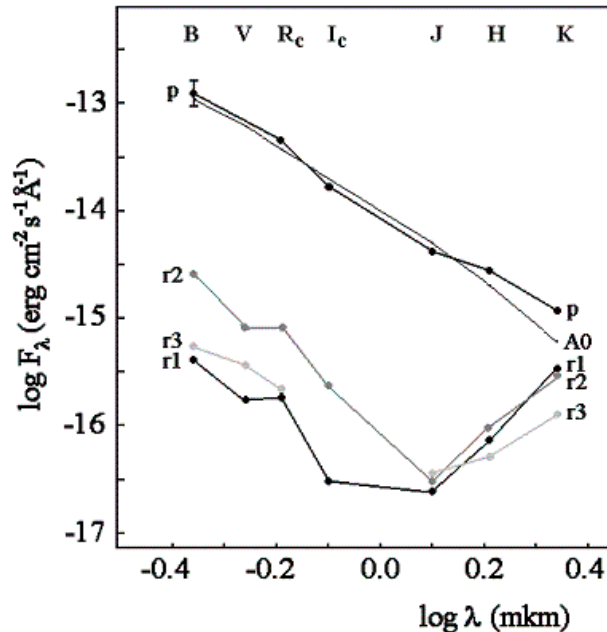


**Figure 7.** The spectral energy distributions determined from photometry. The upper solid curve, marked  $p$ , is the energy distribution of the V445 Pup progenitor, the bars of the  $B$  point correspond to the variability amplitude. The  $JHK$  data are from the 2MASS survey. Interstellar extinction corresponding to  $E(B - V) = 0.51$  was taken into account. The gray curve marked A0 is the energy distribution for an A0V star, plotted for comparison. The three lower curves are energy distributions of the V445 Pup remnant measured at different time: (r1) December 2003; (r2) January 2005; (r3) November 2008. The  $JHK$  observations are from Woudt et al. (2009).

distributions (SEDs) of the progenitor ( $p$ ) and remnant for three different dates: December, 2003, in minimum light after the outburst when its brightness was  $V \approx 20.1$  (r1); January, 2005, in the peak of rebrightening at  $V \approx 18.6$  (r2); and November, 2008, after the rebrightening at  $V \approx 19.2$  (r3). To plot the distributions for the remnant, we used  $JHK$  observations by Woudt et al. (2009) from their Table 2, the closest to our dates. All distributions were dereddened; those for V445 Pup were dereddened with the colour excess  $E(B - V) = 0.51$  (Iijima & Nakanishi 2008), based on calibration of the interstellar NaI doublet equivalent width measured in high-resolution spectra.

We compared our pre-outburst SED with that previously published by Ashok & Banerjee (2003) who find consistency of the SED with an accretion disk model. In the  $JHK$  bands, they used the same 2MASS data, but in the optical  $B$  and  $R$  bands, they used the USNO A2.0 catalog. The USNO A2.0  $R$  magnitude coincides well with our photometry based on Henden’s comparison stars. But the USNO  $B$  value is a half-magnitude brighter than the mean magnitude from our archive observations and is outside the variability range. In Fig. 7 by Ashok and Banerjee (2003), the  $B$  point is located above the straight line fitting the other points. It is clear that it is this deviation in the  $B$  band that caused the choice of the accretion disk model. Additionally, Ashok & Banerjee (2003) used a smaller  $E(B - V)$  value of  $0^m.25$ , derived from the extinction maps by Neckel et al. (1980) and Wooden’s (1970)  $UBV$  photometry of stars in the  $5^\circ \times 5^\circ$  field around V445 Pup. Woudt et al. (2009) reanalyzed the problem of interstellar extinction based on published photometry of open clusters and ascertain that  $E(B - V) = 0.51$  can be the lower limit of Galactic reddening, and the actual value can be between 0.51 and 0.68. They also include circumstellar reddening in their estimates of the star’s absolute magnitude and

luminosity.

Our SED of the V445 Pup progenitor fits that for an A0V star well (A0 in Fig. 7). If we exclude a possible small excess visible in the  $H$  and  $K$  infrared bands, the spectral type may be somewhat earlier. Probably, this excess is the radiation of dust detected by Lynch et al. (2001) in the outburst. But this was not the dust of the surrounding thick disk, assumed to explain the obscuration of the whole system after the outburst. No essential infrared excess is seen in the SED of the progenitor to cause additional circumstellar light absorption and reddening. It is notable that the energy distribution of the progenitor is that of a single star: we do not see any contribution of a cool donor or hot radiation from an accretion disk. Moreover, Kato et al. (2008) demonstrated that the progenitor was too bright to be an accretion disk at the known distance ( $3 \leq d \leq 6.5$  kpc) and with known Galactic interstellar absorption ( $A_V = 1.6$ ) even for the largest reasonable mass accretion rate ( $10^{-6} M_\odot \text{ yr}^{-1}$ ). They note that “it is very unlikely that an accretion disk mainly contributes to the pre-outburst luminosity”. It is evident from our photographic photometry that there were no strong emission lines in the SED of the progenitor which might disturb the plain continuum in such a way as those in the SED of the remnant. But we could not establish any contribution of Balmer absorption or discontinuity of an A0 star due to absence of  $U$ -band observations of the progenitor.

We determined the mean  $\langle B \rangle$  magnitude for V445 Pup to be  $14^{\text{m}}.30$ . Taking into account the A0V energy distribution and the Galactic reddening of  $E(B - V) = 0.51$  (Iijima & Nakanishi 2008), we find  $(B - V)_0 = 0.00$  which corresponds to the star’s reddened values  $B - V = 0^{\text{m}}.51$  and  $\langle V \rangle = 13^{\text{m}}.79$ . With the interstellar reddening of 0.51 and the distance of 5 kpc, we have  $M_V = -1^{\text{m}}.28$ . With the bolometric correction of  $-0.25$  determined for an A0-type star by Straizys (1982), we have  $\log L/L_\odot = 2.54$ . This value is essentially lower than that of 4.34 derived by Woudt et al. (2009). Even with their distance of 8.2 kpc, we find  $M_V = -2^{\text{m}}.36$  and  $\log L/L_\odot = 2.96$ . These luminosity estimates are still too bright to fit models of an accretion disk with a high mass transfer rate. We think that the luminosity of the progenitor was overestimated by Woudt et al. (2009), mostly due to inferring additional circumstellar absorption by an equatorial disk/torus. V445 Pup is an old-population object from its large radial velocity, and its location in the CM diagram is about  $1^{\text{m}}.5 - 2^{\text{m}}.6$  above the RR Lyrae horizontal-branch gap of the globular cluster population.

On the other hand, the energy distributions of the V445 Pup remnant are composite. In the  $H$  and  $K$  bands, this is mostly continuum from cool dust. Woudt et al. (2009) noted two emissions of HeI in the  $0.9 - 2.5 \mu\text{m}$  spectrum taken in January 2004; one of them, at  $1.0820 \mu\text{m}$ , is very strong. In their spectrum, the continuum is present only beginning with  $1.5 \mu\text{m}$ .

Woudt et al. (2009) wrote that V445 Pup was highly reddened in the  $JHK$  bands more than 8 years after the outburst. However, Fig. 2 in their paper shows that all the radiation in the  $K$  band does not belong to an A0 type star highly reddened by the ejected dust envelope. It belongs to the dust envelope itself which consists of two jet-like elongated lobes. No reddened stellar object (such as an A0 type star) is located between the lobes. The  $H$  and  $K$  bands contained mostly the thermal component of  $T = 250$  K, and the intensity of this thermal component gradually declined. The  $J$  band contained the HeI  $\lambda 2.0581 \mu\text{m}$  recombination line with an equivalent width of approximately  $-180 \text{ \AA}$ . The behaviour of the flux in the  $J$  band was different, it did not decline. The figure shows some brightening of the remnant in the  $J$  band simultaneously with the decline in other infrared bands, possibly due to appearance and strengthening of the HeI emission.

In the optical and near-infrared bands, the continuum of the thermal dust component is not found, and we see the recombination lines. In the  $4500 - 7600 \text{ \AA}$  spectrum taken

with the VLT (Woudt et al. 2009), four strong emission lines: [OIII] 4959 Å, HeI 5875 Å, HeI 7065 Å, and the blend [OII] 7319/7330 Å containing four components are present. The HeI and [OIII] lines are spatially resolved. Therefore, our  $BVR_CI_C$  magnitudes and colours do not reflect temperature information, they are formed only by line radiation accidentally hitting the photometric bands. The [OIII] line is at opposite edges of the  $B$  and  $V$  passbands, and the other lines are in the  $R_C$  band. Our  $BVR_CI_C$  observations show brightening of all emission lines in the time ranges from JD 2453004 (r1 in Fig. 7) to JD 2453386 (r2) and subsequent weakening from JD 2453386 (r2) to JD 2454777 (r3).

The changes in the SED due to the outburst in 2000 are radical. We do not see such a blue and bright star as before the outburst. Most investigators, from Henden et al. (2001) to Woudt et al. (2009), write that the binary is obscured by the carbon dust shell ejected in the outburst. However, we do not see such a bright and blue but reddened star either in the deep IR spectra or in the energy distributions. Does any radiation come from under the shell? But there is the ionized gas, ions of [OII] and [OIII]. What is then the source of ionization and excitation?

The light curve of V445 Pup in the optical  $V$  band presented in Fig. 8 looks like a typical light curve of a dust nova having a prolonged dip due to the dust obscuration. Good examples of contemporary dust novae are V1419 Aql, V705 Cas, and V475 Sct. The light curves of these stars can be found in the AAVSO database and in our database at <http://vgoray.front.ru/liststar.htm>. For V445 Pup, such a dip continued approximately since JD  $\sim$  2452200 till JD  $\sim$  2453500. One may assume that, as in other dust novae, the end of this dip and the subsequent star's rebrightening are associated with the dispersion of dust and improvement of visibility of the binary system's remnant. The dispersion of dust leads to temporal strengthening of emission lines in the expanding gaseous envelope. But after that, the tendency of weakening for light from the gaseous envelope continued due to its expansion. This process is typical of classical dust novae in the late stages of outbursts.

## 5 DISCUSSION

There is a consensus that SNe Ia result from the explosion of a carbon-oxygen (CO) white dwarf in a binary system (Meng & Yang, 2010). The cited paper contains a good review of evolutionary ways leading to the SN Ia explosion, with corresponding references to the literature. The first theoretical studies of helium flashes on the surface of a CO white dwarf were performed in the context of SN Ia scenarios. Such dwarfs were members of common envelope binary systems containing a low-mass red giant with a helium core and mass transfer (Hachisu et al. 1989). Depending on the mass transfer rate, helium burning on the surface of a white dwarf may be stable or unstable, with flashes. As a result of helium burning on the surface of a CO white dwarf, its mass gradually increases, exceeds Chandrasekhar limit for the white dwarf mass, and therefore the CO dwarf explodes as a thermonuclear runaway. Hachisu et al. (1989) assume that the progenitor may be observed as a symbiotic star (if the donor is a subgiant) or as an A–F giant (if the donor is a red giant). In the latter case, the mass-receiving component (mass gainer) has the photospheric radius comparable with that of the donor.

Kato et al. (1989) discuss models of a helium nova outburst in a compact binary with direct accretion of helium from a helium star companion which fills its inner critical Roche lobe. In those models, helium shell burning ignites when the density and the temperature in the helium envelope reach critical values. The envelope expands and forms dense stellar wind when it exceeds the critical Roche lobe. When the helium burning ends, the star

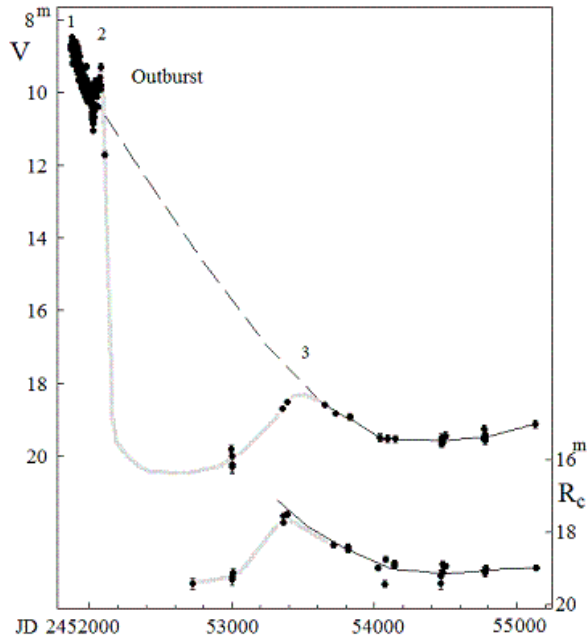


**Figure 8.** The light curve of V445 Pup in the  $V$  band including the 2000 outburst. 1: The primary light maximum; 2: rebrighting before the deep fading; 3: rebrighting in the low state. The gray curve is a dip in the light curve due to carbon dust obscuration. The dashed curve is a typical decay without dust obscuration. The bottom light curve is the post-outburst one in the  $R_C$  band.

returns to the same point in the luminosity–temperature ( $L - T$ ) diagram which was occupied by the progenitor. Helium flashes on the CO white dwarf surface were not considered as a direct cause of the SN explosion.

The appearance of a real helium nova, V445 Pup, showed that these ideas were simplified: dust formation and asymmetry of ejecta were not predicted. Dust forming and dissipation were not considered in the paper by Kato et al. (2008) written after the V445 Pup outburst, they considered only free-free-emission-dominated light curves based solely on the optically thick wind theory.

Recent dynamic calculations by Guillochon et al. (2010) reveal the mechanism of helium ignition on the surface of a white dwarf. With the high accretion rates on the white dwarf surface that range from  $10^{-5}$  to  $10^{-3} M_{\odot} \text{ s}^{-1}$ , the hot helium torus forms, and the accretion stream fails to impact the white dwarf surface. The mass of the torus accumulated during such an event varies between 0.05 and  $0.14 M_{\odot}$ . Due to velocity difference between stream and torus, large-scale Kelvin–Helmholtz instabilities arise along the interface between the two regions which “eventually grow dense knots of material that periodically strike the surface of the primary, adiabatically compressing the underlying helium torus”. The temperature of compressed material increases above a critical temperature ( $2 \cdot 10^9$  K), and then triple- $\alpha$  reactions lead to detonation of the primary’s helium envelope. Moreover, Guillochon et al. (2010) show that shock waves of the detonated envelope tend to concentrate in the focal points within the CO core of the primary. The CO core of a white dwarf can also detonate itself. This kind of detonation of the CO core does not lead to a SN Ia, but such transient events resemble dim type I SNe.

The cited authors used smoothed particle hydrodynamics (SPH) simulations in their calculations. In such an event, the stability of the system depends on the structure of primary and secondary components. However, the particle approximation cannot fully resolve the stream and the helium shell because they have small masses as compared to

the masses of the two components of the binary. To increase the resolution, the authors used a hybrid approach that combined both SPH- and grid-based methods. Grid-based models predict that the donor will survive in such an explosion.

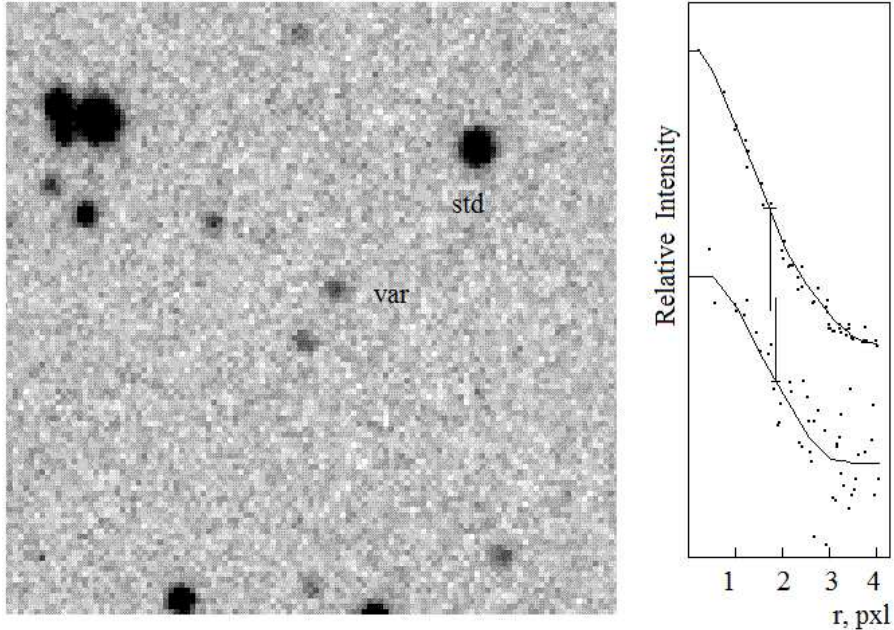


**Figure 9.** An image of V445 Pup taken on 20 October 2009 with the SAO 1-m Zeiss telescope. This is a sum of  $V$  and  $R_C$  frames. This image was obtained on the night with the best seeing ever observed by us,  $\text{FWHM} = 1''.5$ . No elongation is seen in the V445 Pup image (left). To the right, we compare pixel brightness vs. pixel distance from the star center relations for the V445 Pup remnant (bottom) and a nearby comparison star (top). The curves are averaged star image profiles; the vertical lines indicate star image radii at half intensity.

Principally, Guillochon et al. (2010) presented models of merging of a helium star and a CO white dwarf, i.e. a dynamically unstable system in the last orbits before merging. In such an event, the orbital period of the system may be unstable due to angular momentum losses. Theoretical and observational studies of the orbital period stability for a long time interval before the merging event are needed to compare the V445 Pup explosion with the merging model.

Fink et al. (2010) use dynamic calculations to investigate whether an assumed surface helium detonation is capable of triggering a subsequent detonation of the CO white dwarf core. Their calculations were performed for a range of masses of white dwarf cores and masses of helium shells on the white dwarfs' surfaces. The authors find that secondary core detonations are triggered for all of the simulated models, ranging in core mass from  $0.810$  up to  $1.385 M_{\odot}$  with corresponding shell masses from  $0.126$  down to  $0.0035 M_{\odot}$ . The result of the calculations was the following: “as soon as a detonation triggers in a helium shell covering a CO type white dwarf, a subsequent core detonation is virtually inevitable”. For the case of the V445 Pup explosion which began with a helium flash on the surface of the massive CO white dwarf, the white dwarf was destroyed partly or totally. The infrared bipolar nebulosity discovered using adaptive optics may be the debris of the destroyed white dwarf. But V445 Pup is not a dim SN Ia. Having an absolute magnitude  $M_V$  between  $-5.9$  and  $-7.0$  in the light maximum, it did not reach the absolute magnitude level ranging between  $-13$  and  $-14$  for ultra-faint supernovae (Smith et al. 2009), or so

called “supernova impostors”.

What happened in the 2000 explosion event of V445 Pup? Our and other studies established that the progenitor was a hot binary system without a dense dust circumstellar disk. We do not see absorption or emission of such a disk in the energy distribution of the progenitor. The assumption of a cataclysmic binary with the accretion disk is not probable because of high progenitor’s luminosity and an orbital light curve unusual for cataclysmic variables. Indeed, a highly inclined cataclysmic variable has a hump in its light curves caused by visibility of a hot spot on the edge of the accretion disk; the hump is visible only during a half of the orbital period. We assumed that the progenitor was a common envelope binary with a luminous helium donor. The periodic variability suggests a single star with a hot spot on its surface. We know sdB + M type binaries with bright spots on the surfaces of their cool components due to irradiation of ultraviolet flux from an sdB star. However, it is not our case because we do not see a cool companion, the companion was hot. The hypothesis of irradiation of X-rays in a binary with a compact companion is rejected due to absence of an X-ray source associated with the progenitor.

Many observers detected dust formation during the outburst of V445 Pup and the strong dust absorption after the outburst. The observations with adaptive optics reveal a highly collimated bipolar dust and gas ejection located just in the plane of the sky. The small inclination angle of ejection may confirm the presence of an orthogonal dust structure closely aligned to the line of sight and causing the strong extinction observed after the outburst. In the case of merging components, such an orthogonal structure might be a dust disk formed due to angular momentum conservation, but the merging hypothesis needs orbital period instability of the progenitor. Otherwise, this structure should be radially expanding in the equatorial plane. Our optical photometry reflecting changes of fluxes in HeI, [OII], and [OIII] emission lines shows that the dust minimum finished in 2004, leading to strengthening of these lines. Later on, emission line fluxes continued to decrease. This means that the ionizing and exciting radiation comes from outside the place of the explosion, from the dust surroundings. However, no stellar object was seen in the latest adaptive optics image taken in March, 2007.

The absence of a stellar source and the presence of an elongated structure formed only from the ejecta in the frames taken with adaptive optics suggest that components of the system lost their mass and might be destroyed totally or partly. The interpretation of the event as a helium flash is of no doubt. The dynamic theory of such an explosion predicts detonation of the CO white dwarf core and destruction of the white dwarf. Such an explosion will undoubtedly result in the loss of the binary’s common envelope. The remnant may be the core of the helium donor which remains the source of ionizing radiation. In the hypothesis of double detonations, ejecta of the two detonations, the helium shell, and the white dwarf core may be spatially separated.

We analyzed our CCD frames taken with the SAO 1-m reflector. The best-resolution frame with the seeing FWHM =  $1''.5$  was obtained on 20 October 2009. A part of this frame is shown in Fig. 9 (left). The star was faint, and to increase the signal in pixels, we co-added our  $V$  and  $R_C$  frames. In the right panel, the profile of a standard star (top) is compared to the profile of V445 Pup (bottom). These are normalized dependences of pixel counts on the distance between the pixel center and the center of the star image localized by the method of star-profile dispersion minimization. This distance is measured in the units of pixel size,  $0''.44$ . Both images are round, and the image of V445 Pup is marginally resolved. No image elongation is seen, whereas the expected elongation based on Fig. 6 by Woudt et al. (2009) should be 2:1. One should note that the radiation in emission lines was resolved by Woudt et al. (2009) with VLT spectra, and, very probably, it coincides spatially with the lobes seen in the infrared  $K$  band.



In both cases, either CO type white dwarf detonation and destruction or big mass loss from the helium donor, the future SN Ia scenario for V445 Pup becomes impossible. The helium flash accompanied with core detonation seems to be a single event in the life of a white dwarf in the binary system with a helium star. It does not look like a SN Ia. At least, it is too early to discuss the SN Ia scenario for V445 Pup before the possible detection of restored mass exchange in the binary system.

## 6 CONCLUSIONS

We found that V445 Pup progenitor was a binary system. The most probable orbital period was  $0^d650654 \pm 0^d000011$ . The total variability amplitude was  $0^m7$  in the  $B$  band, and the total amplitude of the periodic variability component was  $0^m4$ . Solutions of the light curves with different periods are also possible.

The shape of the progenitor's light curve suggests that it was a common-envelope binary with a spot on the surface of the envelope and with variable surface brightness.

The energy distribution of the progenitor can be successfully fitted with that of a single A0V star with a small infrared excess.

The shape of the light curve after the outburst suggests that the dust absorption minimum finished in 2004. We do not see any stellar remnant either in the optical range or in the infrared. No stellar object, like a reddened A-type star, is visible. We argue that V445 Pup was an event of double detonation, both of the helium envelope of the CO white dwarf and of the CO white dwarf's core, accompanied with the destruction of the common envelope of the binary. In such an event, one of the components of V445 Pup lost a part of its mass, and the other one might be totally destroyed. Thus, V445 Pup, as a remnant of the outburst, cannot be a progenitor of a future SN Ia.

*Acknowledgments:* The authors thank A. Retter and A. Jones for their observations of V445 Pup in outburst provided for our analysis. We also used the Digitized Sky Survey, the SuperCOSMOS Sky Surveys, the United States Naval Observatory (USNO) Image and Catalog Archive, the USNO B1.0 astrometric catalog, and the All Sky Automated Survey (ASAS) data. The information from deep sky surveys is very useful for understanding the nature of astrophysical objects and phenomena. E.A.B., A.V.Zh., and V.P.G. thank Russian Foundation for Basic Research (RFBR) for financial support through grant and No. 07-02-00630. S.Yu.Sh. is grateful to the RFBR for grants No. 08-02-01229 and No. 09-02-90458, to the Slovak Academy of Sciences for the VEGA grant 2/0038/10, and to the Russian Ministry of Education and Science for the grant RNP-2906.

### References:

- Ashok, N.M., & Banerjee, D.P.K., 2003, *Astron. & Astrophys.*, **409**, 1007  
 Deeming, T.J., 1975, *Astrophys. & Space Sci.*, **36**, 137  
 Fink, M., Roepke, F.K., Hillebrandt, W., et al., 2010, *Astron. & Astrophys.*, **514**, A53.  
 Glasner, A., & Livne, E., 2002, AIP Conf. Proc., **637**, 124  
 Guillochon, J., Dan, M., Ramirez-Ruiz, E., & Rosswog, S., 2010, *Astrophys. J.*, **709**, L64  
 Hachisu, I., Kato, M., & Saio, H., 1989, *Astrophys. J.*, **342**, L19  
 Henden, A.A., Wagner, R.M., & Starrfield, S.G., 2001, *IAU Circ.*, No. 7730  
 Iben, I., Jr., & Tutukov, A.V., 1994, *Astrophys. J.*, **431**, 264  
 Iijima, T., & Nakanishi, H., 2008, *Astron. & Astrophys.*, **482**, 865  
 Kato, M., Saio, H., & Hachisu, I., 1989, *Astrophys. J.*, **340**, 509

- Kato, M., Hachisu, I., Kiyota, S., & Saio, H., 2008, *Astrophys. J.*, **684**, 1366
- Kato, T., & Kanatsu, K., 2000, *IAU Circ.*, No. 7552
- Lafler, J. & Kinman, T.D., 1965, *Astrophys. J., Suppl. Ser.*, **11**, 216
- Liller, W., 2001, *IAU Circ.*, No. 7561
- Lynch, D.K., Russell, R.W., & Sitko, M.L., 2001, *Astron. J.*, **122**, 3313
- Lynch, D.K., Rudy, R.J., Mazuk, S., et al., 2004, *IAU Circ.*, No. 8278
- Meng, X. & Yang, W., 2010, *Astrophys. J.*, **710**, 1310
- Neckel, Th., Klare, G., & Sarcander, M., 1980, *Astron. & Astrophys., Suppl. Ser.*, **42**, 251
- Platais, I., Kozhurina-Platais, V., Zacharias, M. I., & Zacharias, N., 2001, *IAU Circ.*, No. 7556
- Smith, N., Ganeshalingam, M., Chornock, R., et al, 2009, *Astrophys. J.*, 697, L49
- Straizys, V., 1982, *Zvezdy s defitsitom metallov (Metal Deficient Stars)*, Vilnius: Mokslas (in Russian)
- Terebizh, V.Yu., 1992, *Analiz vremennykh ryadov v astrofizike (Analysis of Time Series in Astrophysics)*, Moscow: Nauka (in Russian)
- Wagner, R.M., Foltz, C.B., & Starrfield, S.G., 2001, *IAU Circ.*, No. 7556
- Williams, R.E., 1992, *Astron. J.*, **104**, 725
- Wooden, W.H., II, 1970, *Astron. J.*, 75, 324
- Woudt, P.A., Steeghs, D., Karowska, M., et al., 2009, *Astrophys. J.*, 706, 738

Table 1: Colours and magnitudes of comparison stars measured by A. Henden for VSNET

Star #	$V$	$B - V$	$V - R$	$R - I$	$\Delta V$	$\Delta(B - V)$	$\Delta(V - R)$	$\Delta(R - I)$
1	13.351	0.619	0.367	0.355	8	12	11	13
2	13.851	1.565	0.917	0.828	11	31	14	11
3	16.378	0.627	0.347	0.546	101	156	158	189
4	15.707	1.479	0.704	0.831	55	149	71	60
5	14.799	0.586	0.362	0.375	22	36	32	37
6	12.917	0.468	0.322	0.346	6	8	8	9
7	13.887	0.533	0.334	0.322	11	16	16	18
8	14.608	0.532	0.329	0.326	21	31	32	39
9	14.727	0.721	0.446	0.393	25	41	35	40
10	14.558	0.418	0.235	0.208	20	28	32	45
11	14.394	2.324	1.317	1.337	15	97	17	11
12	13.932	1.431	0.817	0.776	11	31	14	12
13	15.190	1.208	0.737	0.731	36	76	46	39
14	14.676	1.210	0.719	0.750	23	50	28	21
15	14.032	1.148	0.664	0.688	12	27	16	14
16	14.062	1.447	0.812	0.802	12	37	16	13
17	14.066	0.355	0.201	0.251	12	17	19	24
18	15.557	1.001	0.604	0.504	45	91	62	64
19	16.082	0.765	0.265	0.495	74	124	118	140
20	15.577	0.723	0.409	0.408	47	77	69	80
21	16.563	0.534	0.407	0.425	113	169	169	198
22	17.151	0.781	0.548	0.922	211	354	313	309

Table 2: Moscow  $B$  magnitudes of V445 Pup

JD hel. -2400000	$B$	$\sigma B$	Plate No.	JD hel. -2400000	$B$	$\sigma B$	Plate No.
40541.555	14.13	0.10	A6833	44257.381	13.95	0.09	A13697
41274.543	14.32	0.02	A7949	44261.369	14.04	0.08	A13722
41274.594	14.38	0.10	A7950	44290.357	14.34	0.11	A13749
41356.357	14.13	0.12	A7962	44315.238	14.18	0.07	A13779
41356.390	14.15	0.15	A7963	44584.501	14.16	0.09	A14157
42719.569	14.59	0.23	A10830	44672.252	14.35	0.09	A14192
42867.242	14.61	0.11	A11009	44673.271	14.34	0.06	A14202
42870.243	13.97	0.15	A11047	44905.601	14.36	0.06	A14665
42871.241	14.64	0.06	A11059	44987.408	14.00	0.06	A14691
42872.242	13.98	0.08	A11071	44988.411	14.39	0.08	A14702
42873.250	14.35	0.09	A11083	44989.379	14.05	0.08	A14717
43160.394	14.09	0.02	A11582	45054.243	14.36	0.07	A14841
43161.413	14.40	0.08	A11593	45326.527	14.16	0.10	A15269
43163.444	14.31	0.05	A11602	45327.464	14.11	0.07	A15275
43167.415	14.21	0.08	A11615	45376.350	14.07	0.10	A15327
43190.348	14.32	0.08	A11861	45396.265	14.40	0.07	A15346
43435.589	14.07	0.06	A12370	45407.241	14.19	0.10	A15356
43850.498	14.28	0.07	A12957	45642.578	14.13	0.04	A15993
43851.501	14.33	0.06	A12963	45699.455	14.41	0.04	A16076
43865.406	14.55	0.07	A12975	45703.433	14.39	0.02	A16089
43898.371	14.53	0.07	A13008	45733.340	14.43	0.10	A16120
43905.327	14.22	0.06	A13026	45734.342	14.11	0.08	A16127
43933.298	14.19	0.05	A13066	47208.316	14.47	0.06	A18258
43935.280	13.97	0.04	A13088	47620.246	14.54	0.08	A18836
43962.241	14.37	0.09	A13110	47835.576	14.32	0.06	A19355
43964.245	14.61	0.03	A13123				

Table 3: Sonneberg  $B$  magnitudes of V445 Pup

JD hel. -2400000	$B$	$\sigma B$	Plate No.	JD hel. -2400000	$B$	$\sigma B$	Plate No.
45779.321	14.23	0.24	GC5336	46826.403	14.54	0.13	GC7618/19/20
46006.624	14.30	0.11	GC5821	46827.400	14.05	0.13	GC7657
46036.581	14.72	0.09	GC5872	46827.416	14.33	0.08	GC7658/59
46059.505	14.46	0.12	GC5910/11	46828.357	14.27	0.13	GC7695/96
46093.444	14.14	0.13	GC5962/63	46828.420	14.47	0.11	GC7698/99
46113.374	14.66	0.09	GC6043/47	46828.454	14.53	0.16	GC7701/02
46116.392	14.12	0.12	GC6083/86	46851.344	14.22	0.19	GC7771/72/73
46385.614	14.07	0.10	GC6603	47566.376	14.28	0.23	GC8869
46387.611	14.02	0.15	GC6645/46	47860.599	14.33	0.19	GC9448/49
46440.464	14.11	0.19	GC6691/92	47861.609	14.46	0.10	GC9477/78
46733.639	14.24	0.08	GC7425	47864.571	14.01	0.07	GC9527/28
46737.649	14.18	0.08	GC7442/43	47943.357	14.54	0.12	GC9541/42
46763.582	14.41	0.05	GC7526/27	48271.476	14.29	0.10	GC9930/31
46763.651	14.48	0.14	GC7531	48273.485	14.34	0.08	GC9973/74
46768.607	14.52	0.05	GC7568	48274.467	14.19	0.12	GC10000/01
46768.617	14.70	0.14	GC7569				

Table 4: Archive photographic magnitudes of V445 Pup from Digital Sky Surveys

JD hel. -2400000	$Mag$	$\sigma$	Band	DSS	Emulsion + Filter	Plate No.
34397.736	14.06	0.08	$B$	POSS	103aO	SO843
34397.815	13.18	0.08	$R$	POSS	103aE	SE842
44333.908	14.29	0.12	$B$	UKST	IIIaJ + GG395	5815
45723.085	13.08	0.05	$I$	UKST	IV N + RG715	8998
46772.806	13.40	0.12	$R$	ESO	IIIaF + RG630	6704
49750.077	13.37	0.08	$R$	UKST	IIIaF + OG590	16496

Table 5: CCD observations of V445 Pup after the outburst

JD hel. -2400000	<i>B</i>	<i>V</i>	<i>R</i>	<i>I</i>	Source <sup>1</sup>
52729.2123	20.76	–	19.45	–	SO
52997.4136	–	–	19.34	19.99	SO
52997.4219	–	19.82	19.25	19.87	SO
53004.3862	–	20.01	19.15	–	SO
53004.3908	20.45	20.23	–	–	SO
53004.3949	20.50	20.29	–	–	SO
53357.5675	–	–	17.56	–	VA
53357.5697	–	–	17.76	–	VA
53357.5741	–	–	17.75	–	VA
53357.5989	19.34	18.69	17.76	–	VA
53386.4143	19.86	18.50	17.53	–	SO
53387.3999	19.58	18.51	17.52	17.71	SO
53652.5755	–	18.58	–	–	SO
53728.5565	19.58	18.84	18.34	–	VA
53827.2144	–	18.90	18.48	–	SO
53827.2172	–	18.93	18.41	–	SO
54035.5993	–	19.49	18.99	20.07	SO
54079.5279	–	–	19.43	–	VA
54091.4894	–	19.52	18.75	–	VA
54146.3261	–	–	18.86	–	SO
54146.3112	–	19.53	18.92	–	SO
54468.4335	20.41	19.49	19.20	–	SO
54468.4365	20.31	19.67	19.42	–	SO
54468.4395	20.31	19.57	–	–	SO
54468.4425	20.23	19.63	–	–	SO
54478.4129	20.62	19.52	18.89	–	SO
54478.4175	20.59	19.52	–	–	SO
54479.4058	20.63	19.62	19.09	–	SO
54499.3535	20.44	19.43	18.94	–	SO
54766.5960	–	19.54	–	–	SO
54766.6014	–	19.46	–	–	SO
54767.5998	–	19.26	19.07	–	SO
54774.5488	–	19.57	19.12	–	SO
54776.5397	20.29	19.53	19.01	–	SO
54778.5388	20.17	19.42	19.00	–	SO
55125.6070	–	19.12	18.98	–	SO

<sup>1</sup>SO: Special Astrophysical Observatory, 1-m Zeiss telescope; VA: SAI Crimean Station, 0.6-m Zeiss telescope.

Table 6: Periods and frequencies revealed

$P$	$\sigma P$	Parameter	$f$ (c/d)	Remark
Deeming		$Ampl./2$		
2.134469	0.00011	0.217	0.468501	$f_0$
1.871862	0.00009	0.217	0.534227	$1 - f_0$
0.679704	0.000012	0.205	1.471229	$1 + f_0$
0.650637	0.000011	0.204	1.536956	$2 - f_0$
0.404207	0.000004	0.185	2.473977	$2 + f_0$
0.393764	0.000004	0.182	2.539658	$3 - f_0$
L-K		$\theta$		
0.650654	0.000011	0.718	1.536914	$2 - f_0$
1.359423	0.000048	0.734	0.735606	d.w. <sup>2</sup>
1.301269	0.000044	0.744	0.768481	d.w.
0.808410	0.000017	0.787	1.236996	d.w.
0.679686	0.000012	0.852	1.471269	$1 + f_0$
0.404207	0.000004	0.844	2.471214	$2 + f_0$

<sup>2</sup>d.w.: a double-wave light curve.